RESEARCH ARTICLE

ADVANCED MATERIALS INTERFACES Open Access

www.advmatinterfaces.de

A Bioinspired Dopamine-Amorphous Calcium Phosphate Coating on Titanium Implant for Osteogenesis and Angiogenesis

Wenjing Wu, Yanhuizhi Feng, and Bing Ni**

Titanium (Ti) is widely used in dental implantation. However, their lack of biological activity causes significant clinical risks associated with immediate loading and early osteointegration failure. Amorphous calcium phosphate (ACP) is reported to be a precursor of bone mineralization. Dopamine (dopa) is well known to possess strong adhesive force in natural mussels. Combining the bio-related advantages of these materials, a dopa-polyacrylic acid (PAA)-ACP hybrid material on the surface of the Ti plate is judiciously fabricated. The biological adhesiveness of dopa to graft it together with PAA onto the surface of Ti is utilized. Then, the dopa-PAA layer serves as a matrix to grow ACP species. The modified interface allows for regulations of bioactivities. MC3T3-E1 osteoblast (MC3T3) cells indeed show improved cell proliferation and adhesion abilities on the Ti with dopa-PAA-ACP coatings compared to those on bare Ti or Ti with only dopa-PAA coating. The osteogenic potential of MC3T3 cells is also considerably upregulated on dopa-PAA-ACP coatings. Moreover, human umbilical vein endothelial cells (HUVECs) on dopa-PAA-ACP coatings show higher levels of angiogenic markers. This report proves that dopa-PAA-ACP composite is a new and simple bioactive titanium coating to facilitate osteogenesis and angiogenesis for dental applications.

1. Introduction

Implant dentures have been one of the main methods of tooth restoration. Titanium (Ti) implants have been most widely used over the decades due to their remarkable mechanical properties and bio-inert ability. However, immediate loading and early bone integration of Ti implants are still important issues troubling the clinical works.[1] Besides, lots of clinical problems like early implant failure appeared with immediate or early loading. Therefore, modifying the interface between Ti and bio-media is highly required, which aims to not only promote osteoblast adhesion, but also induce new vessel formation as well as shorten the osseointegration duration.[2] Simulating the structure and components of bone tissue on the Ti surface is the most convenient way to establish a fast bonding to the host bone for the coatings. Thus, calcium phosphate (CaP) coatings have become a reasonable alternative to enhance titanium implants' osteointegration.[3]

CaP can be classified as hydroxyapatite (HAP), beta-tricalcium phosphate (β-TCP), octacalcium phosphate (OCP), and amorphous calcium phosphate (ACP) (including amorphous calcium orthophosphate phases, poorly defined domains in apatite, amorphous calcium polyphosphates, etc.) based on their chemical composition, crystal structure, and solubility.[4] Among them, HAP is the natural calcium

W. Wu
Department of Prosthodontics
Stomatological Hospital and Dental School of Tongji University
Shanghai Engineering Research Center of Tooth Restoration and Regeneration
Shanghai 200072, China

The ORCID identification number(s) for the author(s) of this article can be found under https://doi.org/10.1002/admi.202301069

[+]Present address: Department of Chemical Engineering, University of Michigan, Ann Arbor, MI 48109, USA

DOI: 10.1002/admi.202301069

Y. Feng
Department of Implantology
Stomatological Hospital and Dental School of Tongji University
Shanghai Engineering Research Center of Tooth Restoration and Regeneration
Shanghai 200072, China
E-mail: 1701385@tongji.edu.cn

B. Ni[+]
Physical Chemistry
University of Konstanz
Universitätsstrasse 10, 78457 Konstanz, Germany
E-mail: bing.ni@uni-konstanz.de

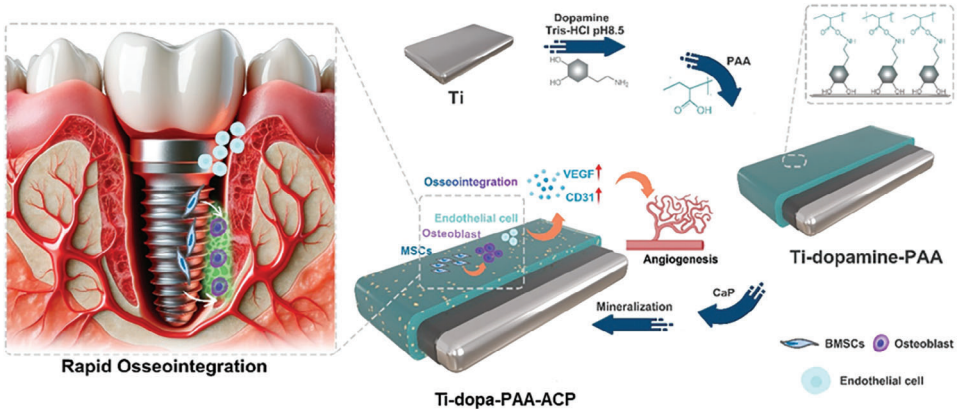

Figure 1. A bioinspired dopa-PAA-ACP coating is fabricated to modify the Ti plate for osseointegation and angiogenesis.

phosphate that exists in teeth, and therefore most frequently used in bone tissue engineering and titanium coatings for its remarkable osteoinductive and osteoconductive properties.[5] However, high crystallinity and stoichiometry of HAP can lead to a relatively slow dissolution rate, which has a negative effect on osteointegration.[6]

ACP, a natural precursor phase of HAP, has been revealed to be a better alternative to HAP. ACP exhibits higher reactivity, solubility, and bioactivity, due to its disordered structure and structural defects.[7] ACP can release calcium and phosphate ions in a physiological context, promoting the growth of HAP crystals in a bio-media and facilitating bone-like apatite development more efficiently.[8] Moreover, ACP was reported to be more beneficial for promoting cell adhesion and osteocalcin production than conventional highly crystalline HAP.[9] At present, ACP has been increasingly widely used in the field of bone tissue regeneration for its outstanding pro-osseogenetic performance.[10] However, how to obtain a solid combination interface between the ACP and the implant is still an urgent problem to be solved.

Learning from nature, dopamine (dopa) is an analog of 3,4-dihydroxy-L-phenylalanine in mussels which plays a crucial role in the tight adhesion of a mussel onto various substrates in spite of a wet environment, including inorganic and organic surfaces such as noble metals, oxides, ceramics, and plastics.[11] Enlightened by the mussel adhesion mechanism, the adhesive application of dopamine has become a focus of research in recent years.[12] Dopamine provides a versatile platform to covalently bond various bioactive molecules for diverse applications.[13] Dopamine exhibited good adhesion properties on Ti surfaces. Besides, it can improve the biocompatibility and hydrophilicity of the Ti surface,[14] thus promoting diverse cell adhesion and spreading. In addition, dopamine is reported to facilitate osteogenic differentiation of osteogenic differentiation of bone marrow-derived mesenchymal stromal cells (BMSCs) by activating osteogenic-related signaling.[15] Furthermore, dopamine is found to promote angiogenesis and have immunomodulatory properties.[13,16] To further enhance the properties of dopamine, Li et al. reported a new method to improve the adhesion of polymers on a metal substrate by grafting polyacrylic acid (PAA)[17] which makes dopamine coating more stable and more durable for long-term operation. Meanwhile, PAA has been used instead of non-collagenous proteins to improve the stability of ACP during biomineralization,[18] thus PAA can simultaneously stabilize dopamine and ACP.

Given the superior biomimetic mineralization ability of ACP, the stabilizing effect of PAA, and the biological viscosity, hydrophilicity, and biocompatibility of dopamine, we fabricated a novel dopa-PAA-ACP coating on Ti implants (**Figure 1**). The coating was proved to have a stable structure, good surface roughness, and great biocompatibility. MC3T3-E1 osteoblast cells seeded on the coating exhibited excellent viability and higher expression of osteogenic genes. Human umbilical vein endothelial cells (HUVECs) cultured on the coating displayed better angiogenesis potential. Overall, the Ti-dopa-PAA-ACP surface can enhance the abilities of cell adhesion, proliferation, osteogenesis, and angiogenesis. Therefore, it is a simple but significant improvement for commercial Ti implants and will be hopeful to improve clinical treatment efficiency with higher bioactivity toward osseointegration and angiogenesis.

2. Results and Discussion

2.1. Morphologies and Structures of the Coatings

As shown in the schematic diagram, we developed a new dopa-PAA-ACP coating with a feasible and simple routine to facilitate the osteoconductive and angiogenesis ability of the Ti surface (Figure 1). Briefly, PAA was first activated by dicyclohexylcarbodiimide (DCC) and N-hydroxysuccinimide (NHS) to form PAA–NHS. Dopamine was then copolymerized with PAA–NHS in an aqueous medium at pH 8.5. The corresponding nuclear magnetic resonance (NMR) chemical signals of PAA–NHS and PAA-NHS-dopamine are shown in Figure S1 (Supporting Information), which shows the compound is successfully grafted. Ti plates were immersed in dopamine and PAA–NHS mixture solutions to get Ti-dopa-PAA. Then, Ti-dopa-PAA plates were immersed in a mineralizing solution to mimic the process of biomineralization for 7 days, and the final product is called Ti-dopa-PAA-ACP. The morphology of the Ti surface was analyzed by SEM after every procedure (**Figure 2A**). After the surface treatments, Ti displayed a porous and rough surface which has been demonstrated to provide excellent mechanical properties for the interface and a 3D structure for cell adhesion.[19] Furthermore, the surface element distributions were examined.

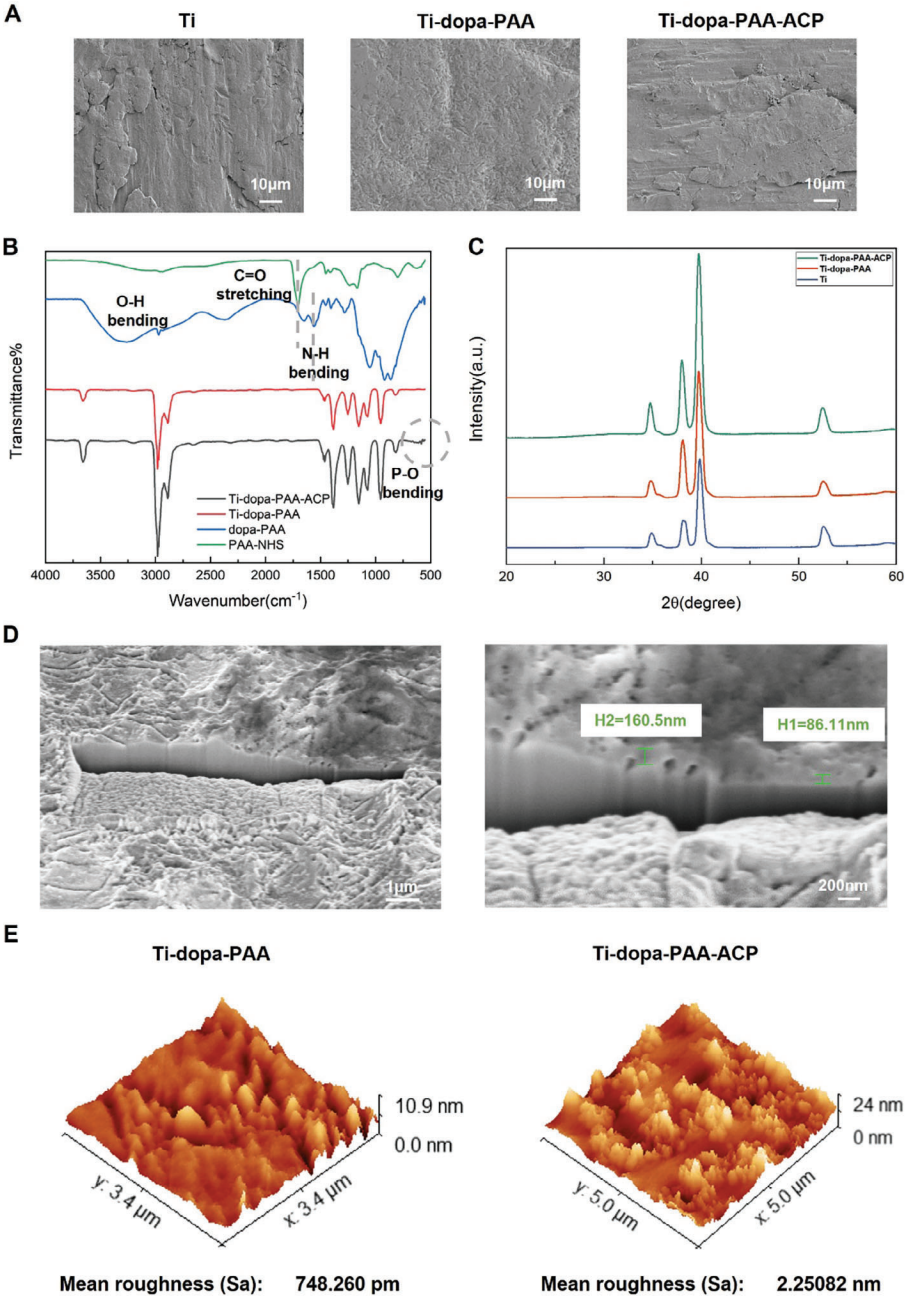

Figure 2. A) Surface SEM images for Ti, Ti-dopa-PAA, and Ti-dopa-PAA-ACP. B) FT-IR spectra analysis of PAA-NHS, dopa-PAA,Ti-dopa-PAA, and Ti-dopa-PAA-ACP. C) XRD spectra of Ti, Ti-dopa-PAA, and Ti-dopa-PAA-ACP samples. D) FIB-SEM images of Ti-dopa-PAA-ACP. E) 3D AFM images of Ti-dopa-PAA and Ti-dopa-PAA-ACP.

Energy dispersive spectroscopy (EDS) analysis revealed that Ti, C, O, N, Ca, and P were detectable on the Ti-dopa-PAA-ACP surface (Figure S2A, Supporting Information), indicating that ACP was successfully synthesized and loaded. EDS mapping further revealed that Ca and P were homogeneously distributed over Ti-dopa-PAA-ACP (Figure S2B, Supporting Information). In order to further explore the chemical composition of the coatings, FT-IR measurements were performed (Figure 2B). PAA-NHS showed a signal in the range between 1500 and 1700 cm^{-1}, which is assigned to the carboxyl group. Besides, the signals at 3300 cm^{-1} in dopa-PAA could be indexed to the O—H group. As for ACP coatings, we can find the P–O bending at 580 cm^{-1} in the Ti-do-PAA-ACP compared with that in the Ti-do-PAA. In addition, XRD was applied to gain a more detailed insight into the phase composition of the dopa-PAA-ACP coating (Figure 2C). Signals at 35,38.4, 40.2, 52.9, and 62.9° were measured for every compound. These signals correspond to the (100), (002), (101), (111), and (002) planes of Ti, respectively. The XRD patterns of

Ti-dopa-PAA and Ti-dopa-PAA-ACP show similar Ti signals. CaP on the surface of Ti-dopa-PAA-ACP could also be inferred as amorphous calcium phosphate rather than crystallized hydroxyapatite. To determine the thickness of the Ti-dopa-PAA-ACP surface layer, the layer was sputtered with gold first and then observed by FIB-SEM. Figure 2D shows the SEM images of the FIB-cuts. Since the surface of Ti is relatively rough and we chose dopamine as the adhesive of PAA and Ti, the coatings show a non-uniform surface. Through FIB-SEM, we can clearly distinguish the upper edge of the titanium as the lower margin of coating thickness, with the sputtered gold edge as the upper margin. We conduct continuous statistics on six points, labeling the thickest and the thinnest data among them accordingly. The approximate thickness in Ti-dopa-PAA-ACP was in a range of 86–160 nm. Furthermore, high-resolution AFM images revealed the roughness of the ACP coatings. In Figure 2E, the roughness with ACP coatings increased dramatically compared with untreated Ti-dopa-PAA. Such an increased roughness would be advantageous for the binding of a variety of proteins, which can combine with selective receptors of osteoblasts to influence osteoblast proliferation and maturation, eventually leading to new bone formation. Moreover, the hydrophilicity of the coatings was measured by static water contact angle (WCA). As shown in Figure S3 (Supporting Information), the WCA on the untreated Ti surface was nearly 95.35°, and the WCA decreased significantly after coated with dopa-PAA and ACP. The mean WCA on Ti-dopa-PAA and Ti-dopa-PAA-ACP surfaces were 27.25 ° and 26.66 ° respectively. Therefore, after coating, the Ti surface became more hydrophilic and therefore more suitable for cell adhesion and proliferation.[20]

2.2. Biocompatibility of the Modified Ti Surfaces

To explore the effects of the coatings on cell biological behaviors including cell adhesion, proliferation, and viability, MC3T3-E1 osteoblast cells were seeded on Ti, Ti-dopa-PAA, and Ti-dopa-PAA-ACP. After 24 h of culture, the morphology and adhesion of MC3T3 cells were detected by SEM and cellular immunofluorescence (ICC) staining. MC3T3 cells on different surfaces all showed good adhesion. The cells adhered to the Ti-dopa-PAA plates displayed a wider cell spreading area and more filopodia and lamellipodia than those on the bare Ti surface, meanwhile, much more extensive MC3T3-E1 cell spreading was observed on the Ti-dopa-PAA-ACP surface (**Figure 3**A). Similarly, ICC images showed cells grew on these surfaces, and the Ti-dopa-PAA-ACP surface exerted more cell projections with randomly arranged cytoskeletal actin filaments which indicated the best attachment (Figure 3B). Moreover, the viability of cells in each group was quantified by Cell counting Kit-8 (CCK8). The results showed that, after culturing for 1, 3, and 5 days, the MC3T3-E1 cells in Ti-dopa-PAA and Ti-dopa-PAA- ACP group showed enhanced proliferation compared with those corresponding to the Ti control group. The difference between Ti-dopa-PAA and Ti-dopa-PAA-ACP was not significant at the beginning, but the OD value of Ti-dopa-PAA-ACP group was significantly higher than that of Ti-dopa-PAA on day 5 (Figure 3C). ICC staining showed the same proliferation trend (Figure S4, Supporting Information). These results showed that dopamine can effectively promote cell adhesion and cell growth, and further ACP modifications can additionally promote cell attachment and proliferation.

2.3. Effect of the Coatings on Osteogenic Differentiation

To evaluate the osteogenic properties of the modified Ti plates, quantitative real-time PCR (qPCR), alkaline phosphatase (ALP) assay, alizarin red staining, and ICC staining were carried out. After several days of osteoinduction, the osteogenic genes of osteopontin (OPN), bone sialoprotein (BSP), and osteocalcin (OCN) were detected by qPCR (**Figure** 4A). In each group, the expression of osteogenic genes was evaluated over time. Cells seeded on the Ti-dopa-PAA-ACP surface expressed higher OPN, BSP, and OCN than those on the other two groups at each time point. On the other hand, Ti-dopa-PAA surface had little effect on osteogenic genes in most time, except that OPN and BSP levels were higher than those in the Ti control in the later stage. Furthermore, ALP staining was also used to test the activity of Ti-dopa-PAA-ACP surfaces in enhancing osteogenic differentiation. As expected, the Ti-dopa-PAA-ACP plate showed a deeper color and larger dyeing area than that in Ti and Ti-dopa-PAA, indicating more significant ALP activities (Figure 4B). Alizarin red staining and the quantitative results indicated significantly more matrix mineralization nodule formation on dopa-PAA-ACP coating than those on dopa-PAA coating and control substrate (Figure 4C,D). Meanwhile, the protein expression levels of Runt-related transcription factor 2 (RUNX2) and OCN were further investigated by ICC staining. Consistently, there was no significant difference between the Ti and the Ti-dopa-PAA group, while the Ti-dopa-PAA-ACP group showed the highest expression of RUNX2 and OCN (**Figure** 5A,B).

We applied different methods to detect early osteogenesis markers (ALP, RUNX2, OPN)[21] and late-stage osteogenesis markers (OCN, BSP),[22] and demonstrated that the Ti-dopa-PAA-ACP surface can promote the entire osteogenic differentiation process of osteoblasts. The mechanism of the Ti-dopa-PAA-ACP promoting osteogenesis can be attributed to the following points. First, the Ti-dopa-PAA-ACP surface is rougher and more hydrophilic, and therefore more suitable for osseointegration by attracting more proteins to promote the adhesion, proliferation, and osteogenesis of osteoblasts.[23] Second, ACP can release Ca^{2+}, which can directly promote bone regeneration.[24] Finally, ACP is more soluble and flexible for reorganization and fusion, and provides an environment for biomimetic mineralization, promoting cell adhesion and osteogenic differentiation. Although some research reported that dopamine has a promoting effect on bone formation,[15,25] similar results were not detected in our experiment, and the osteoinductive effect of dopa-PAA coating on Ti was not evident. This may be due to the concentration of grafted dopamine, which is worth further research in the future.

2.4. Effect of the Coatings on Angiogenesis Ability

Angiogenesis is essential for the osseointegration of implants, by providing the necessary circulating cells, nutrients, and oxygen for the formation and mineralization of the bone matrix.[26] Hence, it is imperative to target relevant biological processes

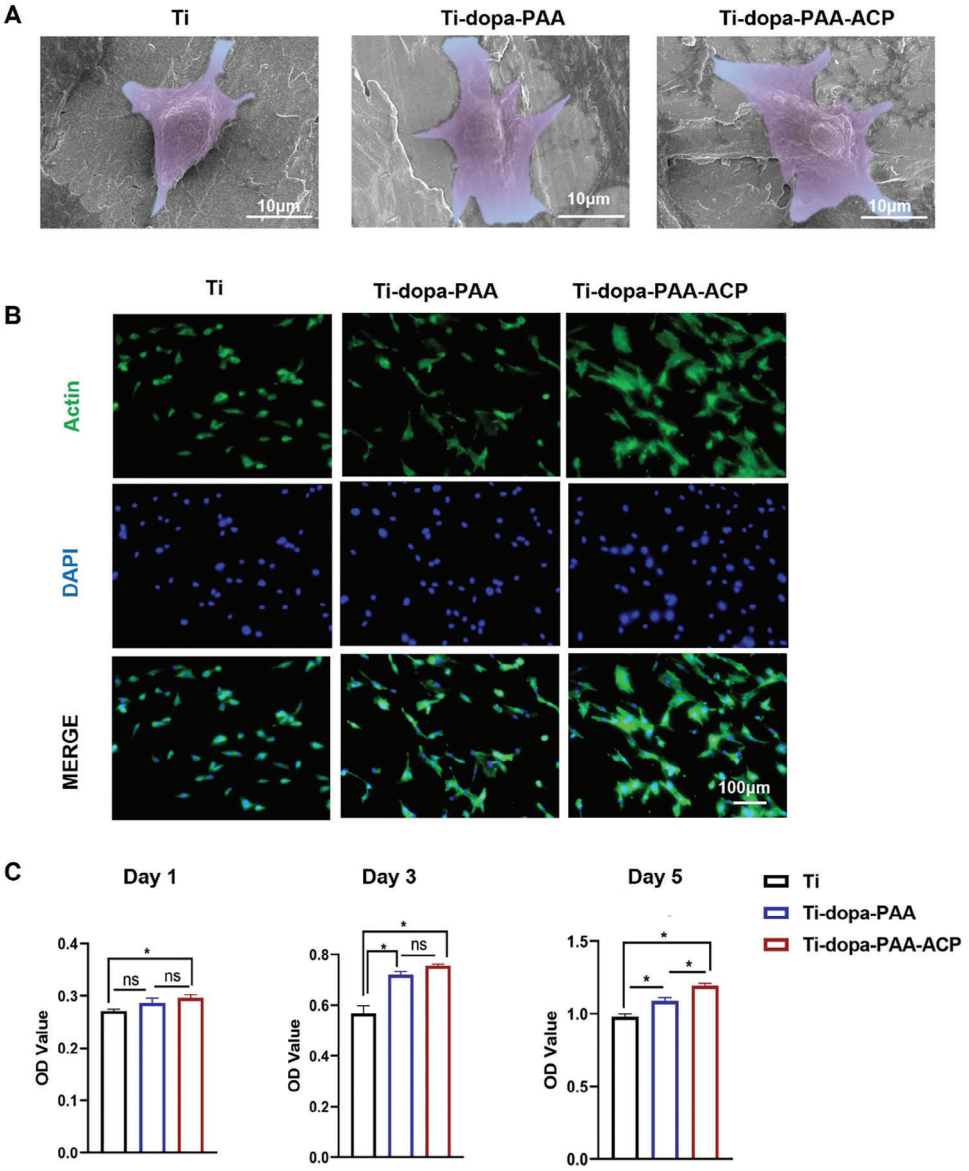

Figure 3. A) SEM images of MC3T3 cells seeded on Ti, Ti-dopa-PAA, and Ti-dopa-PAA-ACP for 24 h. B) Immunofluorescence images of MC3T3 cells cultured Ti, Ti-dopa-PAA, and Ti-dopa-PAA-ACP for 24 h. The scale bar can be applied to every picture. C) Results of Cell Counting Kit-8 (CCK 8) test for MC3T3 cells cultured on Ti, Ti-dopa-PAA, and Ti-dopa-PAA-ACP for 1, 3, 5 days. $^{*}p < 0.05$, ns: not significantly.

to improve the angiogenic properties of titanium implants for enhancing the osseointegration efficacy. To further evaluate the effect of the coatings on angiogenesis ability, we cultured HUVECs on the modified Ti plates. Immunofluorescence staining of biomarkers angiogenesis, vascular endothelial growth factor (VEGF), and CD31[27] showed the strongest fluorescence intensity in the Ti-dopa-PAA-ACP group, while not much difference was observed between the other two groups (**Figure** 6A). At the mRNA level, increased expression of angiogenesis-related genes (CD31 and VEGF*α*) was also detected in the Ti-dopa-PAA-ACP group. However, the Ti-dopa-PAA surface had little effect on the expression of angiogenesis genes (Figure 6B). Similarly, the tubule formation assay displayed the same trend. HUVECs treated with an extraction solution onTi-dopa-PAA-ACP formed more tubes and branches (Figure 6C). Consistent with the reported data,[28] we demonstrated that ACP can accelerate the vascularization process, which is reported to increase by the release of calcium ions.[29] Altogether, Ti-dopa-PAA-ACP plates simultaneously promoted osteogenesis and angiogenesis, which can facilitate vascularized bone formation around the titanium, thereby achieving better and faster osteointegration.

3. Conclusion

Inspired by the mussels in nature, we utilized the excellent physical adhesion properties of dopamine to construct a novel Ti-dopa-PAA-ACP plate in a simple and low-cost way. Dopamine enhanced the hydrophilicity of the substrate, while ACP increased

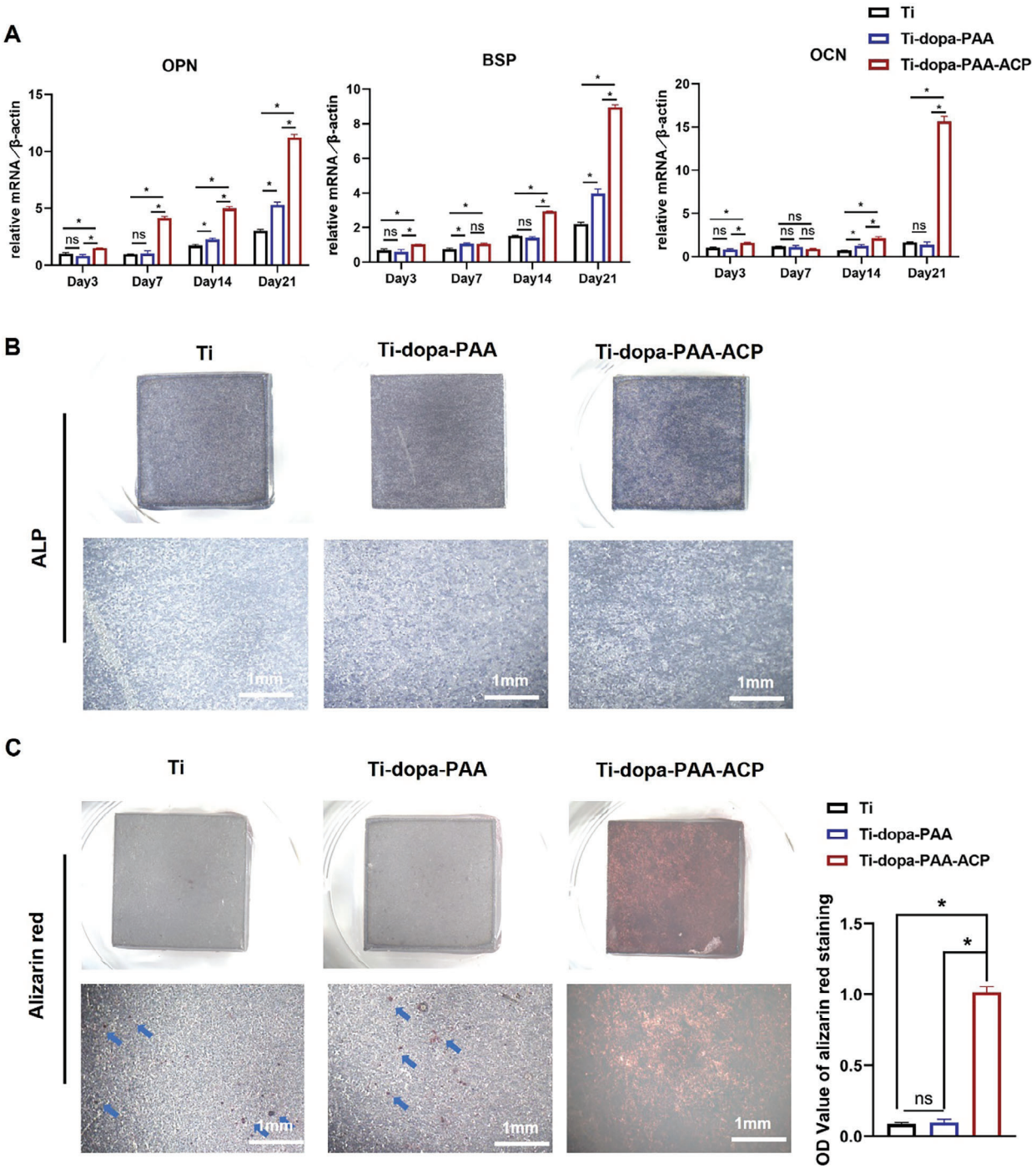

Figure 4. A) Real-time PCR analysis of osteogenic differentiation genes of MC3T3 after culturing for 3, 7, 14, and 21 days on the three groups. $^{*}p < 0.05$, ns: not significantly. B) ALP staining images of MC3T3 cultured on Ti, Ti-dopa-PAA, and Ti-dopa-PAA-ACP for 14 days. C) Alizarin red staining images and quantitative results of MC3T3 cultured on Ti, Ti-dopa-PAA, and Ti-dopa-PAA-ACP for 21 days. The arrows show the calcium nodules.

the surface roughness and the bioactivity, facilitating cell adhesion and proliferation together. Moreover, ACP simultaneously enhanced the osteogenesis of osteoblasts and angiogenesis of endothelial cells, providing a biological basis for rapid osteointegration. Collectively, the Ti-dopa PAA-ACP plate has the advantages of unique design, simple and easy fabrication, stable structure, and outstanding biocompatibility for cell adhesion and proliferation. It can further promote vascularized bone formation, providing a practical and promising strategy to achieve early osseointegration of titanium implants.

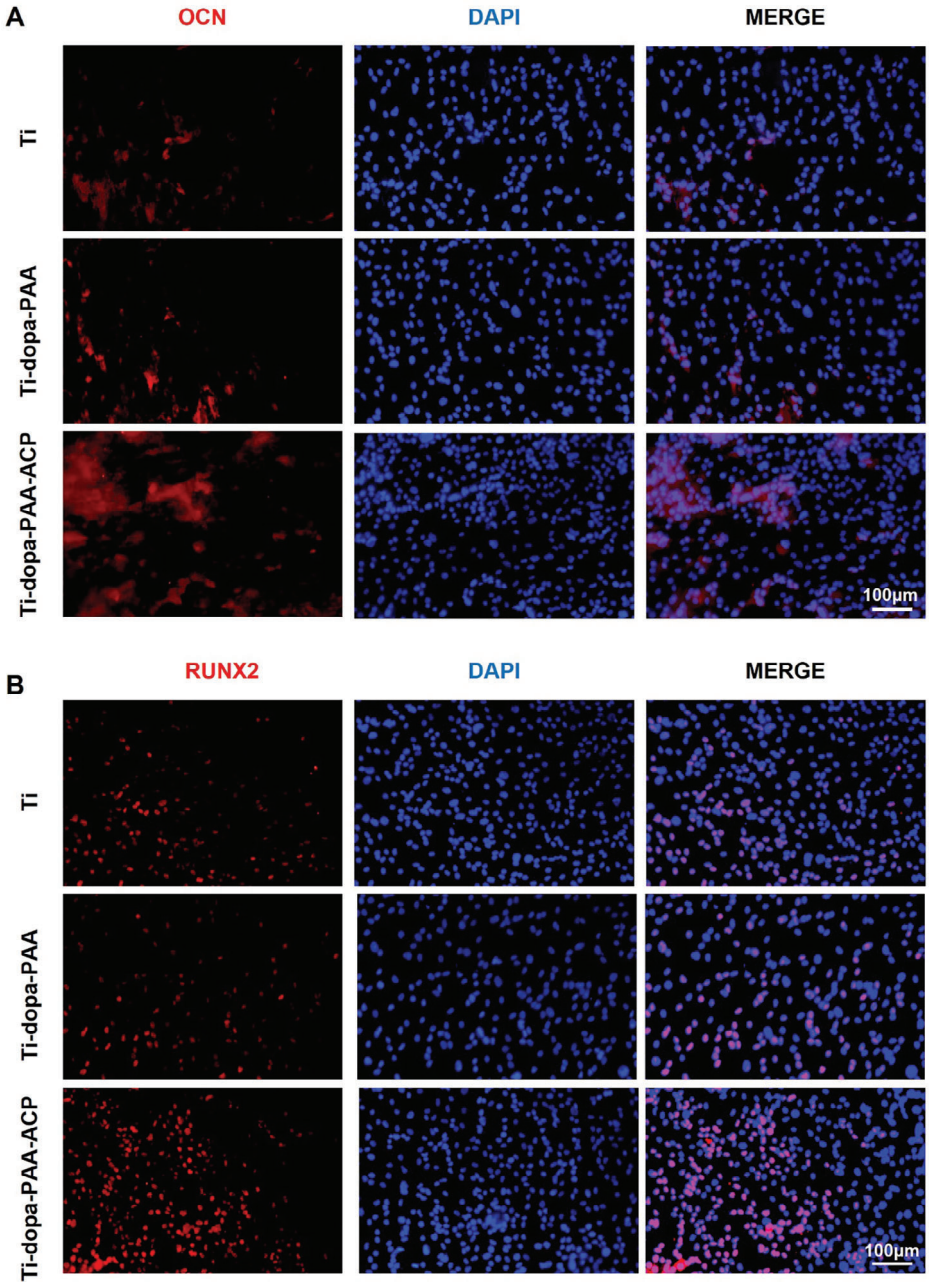

Figure 5. A) OCN immunofluorescence images of MC3T3 cells cultured Ti, Ti-dopa-PAA, and Ti-dopa-PAA-ACP for 14 days after seeding. B) RUNX2 immunofluorescence images of MC3T3 cells cultured Ti, Ti-dopa-PAA, and Ti-dopa-PAA-ACP for 14 days after seeding. The scale bar can be applied to every picture.

4. Experimental Section

Synthesis of PAA-NHS: PAA of 4.5 g (450000), 1.15 g of NHS, and 2.06 g of DCC were successively dissolved in 100 mL of DMF solvent. After stirring for 12 h under ice cooling the reaction mixture was further stirred at 22 °C for 12 h. Crude products were filtrated by filter paper and then dialyzed by water repeatedly for 1 day. The final PAA-NHS product was lyophilized in a lyophilizer for 2 days.

Preparation of Titanium Discs With or Without COATINGS: Dopamine hydrochloride solution was prepared in PBS (20 mL, pH 8.5) and mixed with PAA–NHS. The final concentrations for dopamine hydrochloride and PAA–NHS were 5 and 10 mg mL^{-1}, respectively. Commercial pure titanium plates (10 × 10 × 2 mm, L × W × H) were ultrasonically cleaned in acetone, ethanol, and distilled water, for 30 min successively. After drying with nitrogen, titanium plates were subsequently immersed in dopamine and PAA–NHS mixture solutions at room temperature for 2 days to get dopa-PAA coatings. After 2 days, the dopa-PAA coated titanium plates (labeled as Ti-dopa-PAA) were rinsed thoroughly with deionized water, dried under a nitrogen atmosphere, and stored in vacuum conditions. To get dopa-PAA-ACP coatings, the dopa-PAA coated titanium plates were immersed into 20 mL 1.35 mM $CaCl_2$ solution in HEPES buffer followed by the addition of pAsp (10 μg mL^{-1} in water) and Na_2HPO_4 (1.35 mM in

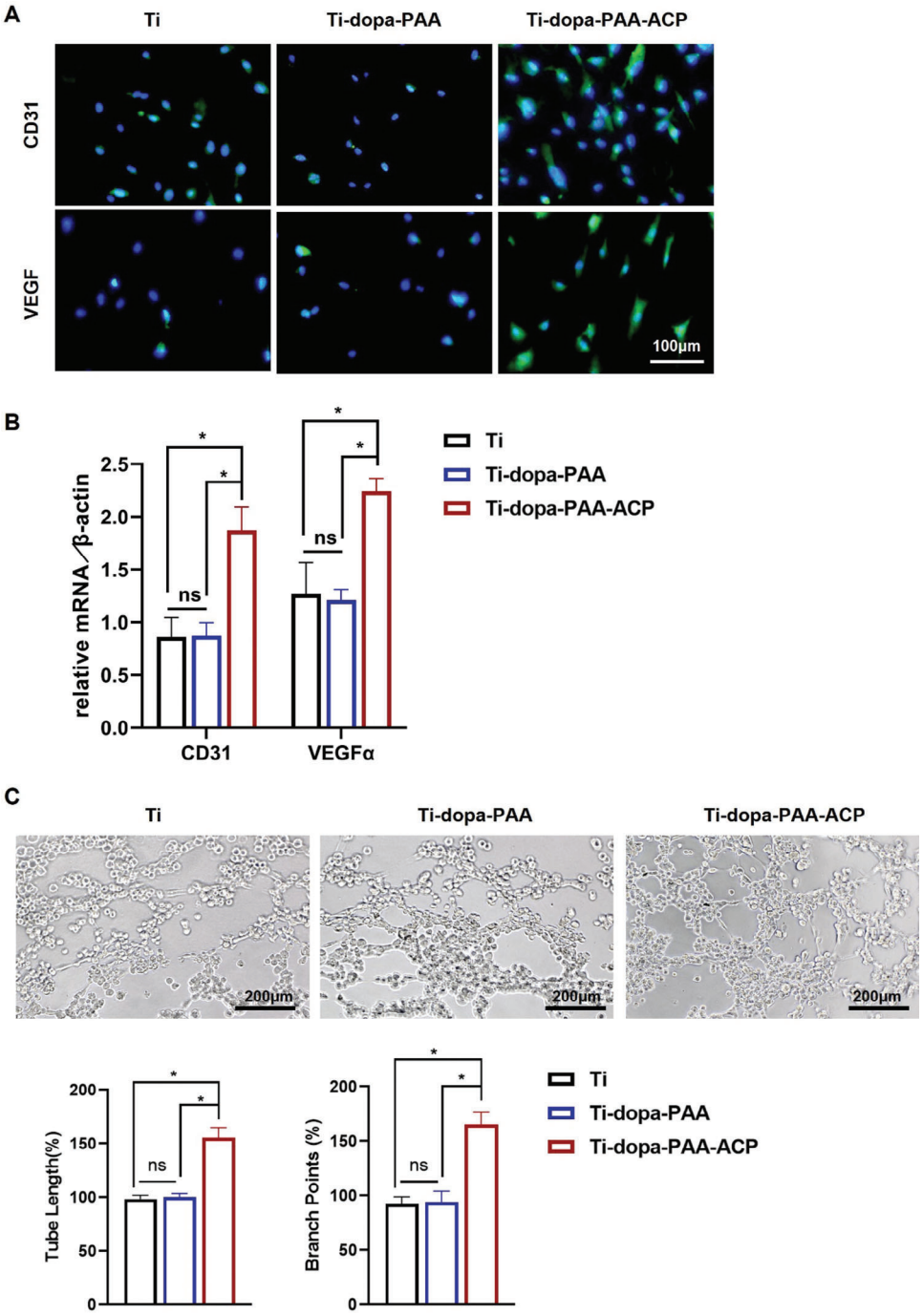

Figure 6. A) CD31 and VEGF immunofluorescence images of HUVECs cultured Ti, Ti-dopa-PAA, and Ti-dopa-PAA-ACP. The scale bar can be applied to every picture. B) Real-time PCR analysis of angiogenesis-related genes of HUVECs after culturing for 3 days on Ti, Ti-dopa-PAA, and Ti-dopa-PAA-ACP. $^{*}p < 0.05$, ns: not significantly. C) Tubule formation assay of HUVECs treated with extraction solution of Ti, Ti-dopa-PAA, and Ti-dopa-PAA-ACP. $^{*}p < 0.05$, ns: not significantly.

water) via a peristaltic pump (2 mL min^{-1}) for 15 min at a pH value of 9. After stirring at 37 °C for 7 days, the plates (labeled as Ti-dopa-PAA-ACP) were washed by H_2O.

Surface Characterization of Dopa-PAA-ACP Coatings: The structure and morphology of coatings were observed by scanning electron microscopy (SEM; Zeiss Gemini500, Germany), energy dispersive spectroscopy (EDS, Inca X-Max, UK), X-ray diffraction analysis (XRD, Rigaku D/max 2500 VB2+/PC, Japan) and Fourier transform infrared (FT-IR) spectra (Bruker spectrometer, IFS 66v/S; Globar (MIR), KBr, DTGS-Detector; Program Opus/IR 3.0.3). Water contact angle measurements were performed by a surface contact angle instrument (DSA25, Krüss, Germany).

Thickness or Toughness of dopa-PAA-ACP Coatings: Focused ion beam-scanning electron microscopy (FIB-SEM; Zeiss, Germany) was employed to detect the thickness of *dopa-PAA-ACP* coatings. Atomic force microscopy (AFM; JPK, Japan) was applied to measure the 3D morphology and roughness.

Cell Culture: The MC3T3-E1 and HUVEC cell lines used for the in vitro study, were purchased from the National Collection of Authenticate Cell Cultures. The MC3T3-E1cells were cultured in αMEM (HyClone, USA) containing 10% fetal bovine serum (BI, Israel). The HUVECs were cultured in DMEM (high glucose, HyClone) containing 10% fetal bovine serum (BI). The medium was changed every other day. Once 80 to 90% confluence was reached, the cells were detached with 0.25% trypsin (HyClone) and replated at a dilution of 1:3. All the cells were incubated at 37 °C within an atmosphere of 95% humidity and 5% CO_2.

Cell Viability Test: MC3T3 cells were separately seeded on Ti, Ti-dopa-PAA, and Ti-dopa-PAA-ACP at a density of 1×10^4 per well in 24-well plates. After 1 day, 3 days, and 5 days of culture, cell viability was assayed using a Cell counting Kit-8 (CCK8; Beyotime, China) according to the manufacturer's instructions.

Cell Adhesion Test: These 1×10^4 MC3T3 cells were plated to Ti, Ti-dopa-PAA, and Ti-dopa-PAA-ACP respectively. After 1 day, 3 days, and 5 days of culture, cells were fixed with 4% PFA for 20 min. They were then stained with Actin-FITC (Beyotime) for 40 min and DAPI for 5 min at 37 °C. After washing with PBS, the cells and materials were observed under confocal laser scanning microscopy (Nikon, Japan). As for SEM observation, 1×10^4 MC3T3 cells were seeded in each group and cultured for 24 h. Then, cells were washed with PBS and fixed with 2.5% glutaraldehyde for 6 h and serially dehydrated with an increasing ethanol gradient, air-dried within a hood, and sputtered with gold prior to imaging under SEM.

ALP and Alizarin Red Staining: The MC3T3 cells were plated to Ti, Ti-dopa-PAA, and Ti-dopa-PAA-ACP at a density of 5×10^4 cells per well and cultured in osteogenic medium. The medium was changed every 3 days. On day 14, an Alkaline phosphatase (ALP) stain kit (Beyotime) was applied to identify the activity of osteogenic cells. On day 21, alizarin red (Sigma) staining was performed. For both staining, the cells were fixed by 4% PFA and cleaned by PBS. The incubating solution was added to plates for 20 min and then cleaned by PBS. The images were captured by microscopy (Olympus, Japan). In addition, to quantify matrix mineralization, the alizarin red stained cultures were incubated with 10% cetylpyridinium chloride for 30 min at room temperature to solubilize and release calcium-bound alizarin red into solution. The absorbance of the solution was measured at 562 nm using a microplate reader and then statistically analyzed.

Quantitative Real-Time PCR Analysis: Total RNA was extracted using the RNAiso Plus reagent (TaKaRa Bio, Japan), reverse transcribed using a PrimeScript RT reagent kit (TaKaRa Bio), and then subjected to qPCR analysis using SYBR Mix (Yeasen, Shanghai, China) and a LightCycler System (Roche, Switzerland). Fold changes in mRNA were calculated by the $2-\Delta\Delta Ct$ method after normalization to the expression of β-actin.

Cellular Immunofluorescence Staining (ICC): After conditional culturing, the cells were fixed in 4% PFA for 15 min and permeabilized with 0.5%Triton X-100 for 10 min followed by washing in PBS. After that, the cells were blocked in FBS for 1 h at room temperature, and incubated with the primary antibody overnight at 4 °C. After being rinsed three times with PBS, the secondary antibody was incubated for 1 h. Finally, the cells were stained with DAPI (Beyotime) mounted with an antifade reagent. Images were captured by a confocal laser scanning microscopy (Nikon). The primary antibodies were RUNX2 (ab236639, Abcam, UK), OCN (DF12303, Affinity, China), CD31 (ab76533, Abcam), and VEGF (AF5131, Affinity).

Tubule Formation Assay: To detect the angiogenesis of HUVECs in vitro, the Matrigel matrix (Yeasen, China) was used according to the manufacturer's protocol. Briefly, Matrigel of 50 µL was added to a 96-well plate using precooled pipette tips. The Matrigel was placed in the incubator at 37 °C for about 30 min to solidify. Then, HUVECs (1.5×10^5 cells) were seeded on the surface of Matrigel, and 50 µL of different material extracts (coated Ti plates immersed in DMEM with 10% FBS for 48 h) were added. Culturation for 4 h, the cells were observed via microscope. The number of junctions and total length of tubes were calculated using Image J software.

Statistical Analysis: The data are represented as the mean ± SEM of independent samples. All statistical analyses were performed with SPSS software (Version 20.0) by Student's t-test or one-way ANOVA. A p-value < 0.05 was considered statistically significant.

Supporting Information

Supporting Information is available from the Wiley Online Library or from the author.

Acknowledgements

This work was financially supported by the National Natural Science Foundation of China (Grant 82301152), Shanghai Pujiang Program (Grant 22PJD081), the Fundamental Research Funds for the Central Universities (Grant 22120220640).

Open access funding enabled and organized by Projekt DEAL.

Conflict of Interest

The authors declare no conflict of interest.

Data Availability Statement

The data that support the findings of this study are available in the supplementary material of this article.

Keywords

amorphous calcium phosphate, angiogenesis, dopamine, osteogenesis, titanium

Received: December 17, 2023
Revised: March 23, 2024
Published online: April 18, 2024

[1] D. D. Bosshardt, V. Chappuis, D. Buser, *Periodontol 2000* **2017**, *73*, 22.
[2] E. K. Papynov, O. O. Shichalin, A. A. Belov, I. Y. Buravlev, V. Y. Mayorov, A. N. Fedorets, A. A. Buravleva, A. O. Lembikov, D. V. Gritsuk, O. V. Kapustina, Z. E. Kornakova, *J Funct Biomater* **2023**, *14*, 259.
[3] G. Desante, I. Pudełko, M. Krok-Borkowicz, E. Pamuła, P. Jacobs, A. Kazek-Kęsik, J. Nießen, R. Telle, J. Gonzalez-Julian, K. Schickle, *ACS Appl. Mater. Interfaces* **2023**, *15*, 21699.
[4] N. Eliaz, N. Metoki, *Materials (Basel)* **2017**, *10*, 10040334.
[5] a) D. Acharjee, S. Mandal, S. K. Samanta, M. Roy, B. Kundu, S. Roy, P. Basak, S. K. Nandi, *ACS Biomater. Sci. Eng.* **2023**, *9*, 4673; b) I. Ielo, G. Calabrese, G. De Luca, S. Conoci, *Int. J. Mol. Sci.* **2022**, *23*, 9721.
[6] M. P. Bernardo, B. C. R. da Silva, A. E. I. Hamouda, M. A. S. de Toledo, C. Schalla, S. Rütten, R. Goetzke, L. H. C. Mattoso, M. Zenke, A. Sechi, *Sci. Rep.* **2022**, *12*, 2333.
[7] S. Santhakumar, A. Oyane, M. Nakamura, K. Koga, S. Miyata, K. Muratsubaki, H. Miyaji, *Mater Sci Eng C Mater Biol Appl.* **2020**, *116*, 111194.
[8] W. Yu, T. W. Sun, C. Qi, Z. Ding, H. Zhao, F. Chen, D. Chen, Y. J. Zhu, Z. Shi, Y. He, *ACS Appl. Mater. Interfaces* **2017**, *9*, 3306.

[9] W. Cárdenas-Aguazaco, B. Camacho, E. Y. Gómez-Pachón, A. L. Lara-Bertrand, I. Silva-Cote, *Pharmaceutics* **2023**, *15*, 2529.
[10] a) Y. Chen, Y. Zhang, X. Chen, J. Huang, B. Zhou, T. Zhang, W. Yin, C. Fang, Z. Yin, H. Pan, X. Li, W. Shen, X. Chen, *Adv. Sci. (Weinh)* **2023**, *10*, e2304216; b) M. Su, C. Li, S. Deng, L. Xu, Z. Shan, Y. Xing, X. Li, Y. Li, X. Liu, X. Zhong, K. Chen, S. Chen, Q. Liu, X. Wu, Z. Chen, S. Wu, Z. Chen, *ACS Appl. Mater. Interfaces* **2023**, *15*, 58166; c) Y. Feng, D. Wu, J. Knaus, S. Kessler, B. Ni, Z. Chen, J. Avaro, R. Xiong, H. Colfen, Z. Wang, *Adv. Healthcare Mater.* **2023**, *12*, e2203411.
[11] a) Y. Shi, R. Jiang, M. Liu, L. Fu, G. Zeng, Q. Wan, L. Mao, F. Deng, X. Zhang, Y. Wei, *Mater Sci Eng C Mater Biol Appl* **2017**, *77*, 972; b) H. Lee, S. M. Dellatore, W. M. Miller, P. B. Messersmith, *Science* **2007**, *318*, 426; c) P. L.e Tran, T. T. Pham, H. S. Lee, S. Hahn, J. U. Choi, J. H. Kim, H. L. Jiang, S. Yook, J. H. Jeong, *J Control Release* **2023**, *364*, 37; d) S. Tan, Y. Qiu, H. Xiong, C. Wang, Y. Chen, W. Wu, Z. Yang, F. Zhao, *Mater Today Bio* **2023**, *23*, 100843.
[12] a) M. Renner-Rao, F. Jehle, T. Priemel, E. Duthoo, P. Fratzl, L. Bertinetti, M. J. Harrington, *ACS Nano* **2022**, *16*, 20877; b) Y. Li, J. Cheng, P. Delparastan, H. Wang, S. J. Sigg, K. G. DeFrates, Y. Cao, P. B. Messersmith, *Nat. Commun.* **2020**, *11*, 3895.
[13] W. Zhang, L. Liu, H. Zhou, C. He, X. Yang, J. Fu, H. Wang, Y. Liu, Y. Zheng, *Mater. Des.* **2023**, *232*, 112151.
[14] a) L. Meng, C. Huang, X. Liu, H. Qu, Q. Wang, *Front Bioeng Biotechnol* **2023**, *11*, 1167340; b) S. Wang, Z. Wu, Y. Wang, H. Hong, L. Zhang, Z. Chen, P. Zhang, Z. Chen, W. Zhang, S. Zheng, Q. Li, W. Li, X. Li, H. Qiu, J. Chen, *Regen Biomater* **2023**, *10*, rbac082.
[15] H. Wang, C. Lin, X. Zhang, K. Lin, X. Wang, S. G. Shen, *ACS Appl. Mater. Interfaces* **2019**, *11*, 7615.
[16] X. Su, Z. Lyu, Y. Wu, Y.-H. Gu, S. Huo, C. Zhou, *Mater. Des.* **2023**, *225*, 111552.
[17] L. J. Duan, Y. Liu, J. Kim, D. J. Chung, *J. Appl. Polym. Sci.* **2013**, *130*, 131.
[18] a) S. Yao, X. Lin, Y. Xu, Y. Chen, P. Qiu, C. Shao, B. Jin, Z. Mu, N. Sommerdijk, R. Tang, *Adv. Sci. (Weinh)* **2019**, *6*, 1900683; b) N. Li, W. Cui, P. Cong, J. Tang, Y. Guan, C. Huang, Y. Liu, C. Yu, R. Yang, X. Zhang, *Bioact Mater* **2021**, *6*, 2303.
[19] G. Mendonça, D. B. Mendonça, F. J. Aragão, L. F. Cooper, *Biomaterials* **2008**, *29*, 3822.
[20] F. Rupp, R. A. Gittens, L. Scheideler, A. Marmur, B. D. Boyan, Z. Schwartz, J. Geis-Gerstorfer, *Acta Biomater.* **2014**, *10*, 2894.
[21] a) Z. Jiang, H. Wang, K. Yu, Y. Feng, Y. Wang, T. Huang, K. Lai, Y. Xi, G. Yang, *ACS Appl. Mater. Interfaces* **2017**, *9*, 34674; b) C. Granéli, A. Thorfve, U. Ruetschi, H. Brisby, P. Thomsen, A. Lindahl, C. Karlsson, *Stem Cell Res.* **2014**, *12*, 153; c) D. S. Amarasekara, S. Kim, J. Rho, *Int. J. Mol. Sci.* **2021**, *22*, 2851.
[22] a) R. J. Miron, Y. F. Zhang, *J Dent Res.* **2012**, *91*, 736; b) A. Rutkovskiy, K. O. Stensløkken, I. J. Vaage, *Med Sci Monit Basic Res.* **2016**, *22*, 95.
[23] a) J. Xia, Y. Yuan, H. Wu, Y. Huang, D. A. Weitz, *Biomaterials* **2020**, *248*, 120014; b) W. E. Yang, H. H. Huang, *J Dent Res.* **2021**, *100*, 1186; c) C. Liu, Y. Li, J. Wang, C. Liu, W. Liu, X. Jian, *Molecules* **2018**, *23*, 1643.
[24] Z. Li, X. Zhang, J. Ouyang, D. Chu, F. Han, L. Shi, R. Liu, Z. Guo, G. X. Gu, W. Tao, L. Jin, J. Li, *Bioact Mater* **2021**, *6*, 4053.
[25] X. Yang, Q. Wang, Y. Zhang, H. He, S. Xiong, P. Chen, C. Li, L. Wang, G. Lu, Y. Xu, *Colloids Surf B Biointerfaces* **2023**, *224*, 113196.
[26] a) Z. Liu, H. Ding, L. Qi, J. Wang, Y. Li, L. Liu, G. Feng, L. Zhang, *ACS Appl. Mater. Interfaces* **2023**, *15*, 52276; b) D. Sang, K. Wang, X. Sun, Y. Wang, H. Lin, R. Jia, F. Qu, *ACS Appl. Mater. Interfaces* **2021**, *13*, 9604.
[27] N. Ferrara, *Endocr Rev.* **2004**, *25*, 581.
[28] a) K. F. Eichholz, P. Pitacco, R. Burdis, F. Chariyev-Prinz, X. Barceló, B. Tornifoglio, R. Paetzold, O. Garcia, D. J. Kelly, *Adv. Healthcare Mater.* **2023**, e2302057; b) X. Yuan, T. Wu, T. Lu, J. Ye, *ACS Biomater. Sci. Eng.* **2023**, *9*, 5761.
[29] Y. Mo, W. He, S. Hu, H. Guo, S. Li, J. Zhang, X. Wang, *J. Biomater. Appl.* **2023**, 8853282231216546.